Phase correction of electromagnetic coupling effects in cross-borehole EIT measurements

2015 Meas. Sci. Technol. 26 015801

(http://iopscience.iop.org/0957-0233/26/1/015801)

OPEN ACCESS
IOP Publishing
Measurement Science and Technology
Meas. Sci. Technol. **26** (2015) 015801 (11pp)
doi:10.1088/0957-0233/26/1/015801

Phase correction of electromagnetic coupling effects in cross-borehole EIT measurements

Y Zhao[1], E Zimmermann[1], J A Huisman[2], A Treichel[2], B Wolters[1], S van Waasen[1] and A Kemna[3]

[1] ZEA-2 Electronic Systems, Forschungszentrum Jülich GmbH, 52425 Jülich, Germany
[2] IBG-3 Agrosphere, Forschungszentrum Jülich GmbH, 52425 Jülich, Germany
[3] Department of Geodynamics and Geophysics, University of Bonn, 53115 Bonn, Germany

E-mail: e.zimmermann@fz-juelich.de

Received 20 March 2014, revised 14 September 2014
Accepted for publication 28 October 2014
Published 24 November 2014

Abstract

Borehole EIT measurements in a broad frequency range (mHz to kHz) are used to study subsurface geophysical properties. However, accurate measurements have long been difficult because the required long electric cables introduce undesired inductive and capacitive coupling effects. Recently, it has been shown that such effects can successfully be corrected in the case of single-borehole measurements. The aim of this paper is to extend the previously developed correction procedure for inductive coupling during EIT measurements in a single borehole to cross-borehole EIT measurements with multiple borehole electrode chains. In order to accelerate and simplify the previously developed correction procedure for inductive coupling, a pole–pole matrix of mutual inductances is defined. This consists of the inductances of each individual chain obtained from calibration measurements and the inductances between two chains calculated from the known cable positions using numerical modelling. The new correction procedure is successfully verified with measurements in a water-filled pool under controlled conditions where the errors introduced by capacitive coupling were well-defined and could be estimated by FEM forward modelling. In addition, EIT field measurements demonstrate that the correction methods increase the phase accuracy considerably. Overall, the phase accuracy of cross-hole EIT measurements after correction of inductive and capacitive coupling is improved to better than 1 mrad up to a frequency of 1 kHz, which substantially improves our ability to characterize the frequency-dependent complex electrical resistivity of weakly polarizable soils and sediments *in situ*.

Keywords: electrical impedance tomography, spectral induced polarization, phase error, electromagnetic coupling, cable coupling, electrode chain, borehole measurement

(Some figures may appear in colour only in the online journal)

1. Introduction

Electrical Impedance Spectroscopy (EIS) measurements, also known as Spectral Induced Polarization (SIP), have established promising relationships between the complex electrical resistivity and important hydrogeological properties, such as pore geometry, pore fluid chemistry and mineral surface properties (see e.g. Vanhala 1997, Slater and Lesmes 2002, Binley *et al* 2005). Several studies have reported that the phase angle of the complex electrical resistivity varies with the frequency (Binley *et al* 2005, Leroy *et al* 2008, Zimmermann *et al* 2008, Breede *et al* 2012) and advanced

impedance spectrometers have been developed to measure the complex electrical resistivity with sufficient accuracy in the mHz to kHz frequency range (Zimmermann *et al* 2008). Spectral Electrical Impedance Tomography (EIT) is a new method which combines the diagnostic potential of SIP with the imaging capability of tomography (see e.g. Kemna *et al* 2000, Flores Orozco *et al* 2012). To image the spectral phase response of low-polarizable soil and sediment samples, a spectral EIT data acquisition system was developed by Zimmermann *et al* (2008), which reaches a phase accuracy of better than 1 mrad at 1 kHz in the laboratory under optimal conditions. Recently, electrode chains and logging tools have been developed to allow borehole EIT measurements in the mHz to kHz range using the EIT data acquisition system described in Zimmermann *et al* (2008).

Accurate borehole EIT measurements above frequencies of ~10 Hz require the consideration of electromagnetic (EM) coupling between the wires for current injection and potential measurement. The theoretical calculation of EM coupling between grounded wires on the surface of the earth has previously been treated in some detail (e.g. Sunde 1968, Wynn and Zonge 1977, Wait 1984, Ward and Hohmann 1988). In these contributions, the mutual impedance that represents the total response from the earth and the wires was split into two parts. The first part describes the complex electrical resistivity of the earth and the second part describes the inductive coupling between the electrical wires, which only depends on the geometry of the wire layout. However, the main problem with the application of these theoretical approaches to borehole EIT measurements is the need to know the position of adjacent wires in borehole electrode chains with sufficient accuracy. In previous work, we solved this problem for measurements with a single borehole electrode chain using a method based on calibration measurements (Zhao *et al* 2013). This calibration must be done only once because it does not depend on the cable layout of the field measurement.

EM coupling in cross-hole EIT measurements with multiple borehole electrode chains was not yet considered in great detail. In this case, inductive coupling cannot be corrected by only using calibration data because the coupling between different electrode chains depends on the cable layout of the field measurement. This part of the inductive coupling must be calculated for each measurement. To improve applicability of corrections of inductive coupling, there is clearly a need for an effective framework to jointly consider calibration measurements and numerical calculations based on cable geometry to correct EIT measurements with arbitrary electrode configurations using one or multiple borehole electrode chains. Thus, we aim to i) characterize inductive coupling in cross-borehole EIT measurements with multiple electrode chains and ii) develop an efficient correction procedure that combines calibration measurements and numerical modelling to obtain accurate cross-borehole EIT measurements. In order to verify the extended correction procedures, EIT measurements were performed under controlled conditions in a water-filled pool. In addition, the correction procedures were applied to actual borehole EIT measurements.

2. EIT borehole measurement setup

The EIT system used in this study is an extension of the EIT laboratory system (Zimmermann *et al* 2008, 2010) that was designed to make accurate impedance measurement using two electrodes for current injection and two electrodes for potential measurement. The system has 40 channels that can be used for current injection and potential measurement at each electrode. To achieve this, each channel is connected with a multi-functional electrode module that consists of an integrated relay for current injection and an amplifier for potential measurement. In order to make borehole EIT measurements, electrode chains with 8 electrode modules and an electrode separation of 1 m were built. The electrode modules are connected to an adapter box close to the EIT data acquisition system using a 25 m long multicore cable that consists of 16 shielded, twisted wire pairs. To ensure a good electrical contact with the surrounding medium, we used brass ring electrodes with a diameter of 42 mm and a height of 10 mm (Zhao *et al* 2013).

The system can be used for field EIT measurements with two or more borehole electrode chains and all possible electrode configurations can be measured. For the purpose of characterizing inductive coupling, electrode configurations can be divided into two general cases (figure 1). In the first case, the current electrodes and the potential electrodes are located in the same borehole (figure 1(*a*)). In the second case, one or more of the current and potential electrodes are placed in a different borehole. Electrode configurations of the second type include cross-borehole dipole-dipole configurations (figure 1(*b*)), unconventional electrode configurations with one electrode in a different borehole (figure 1(*c*)) and classic cross-borehole electrode configurations with current and potential electrodes in both boreholes (figure 1(*d*)). Because of the relatively long electrical wires used in borehole EIT measurements, electromagnetic coupling effects that substantially reduce the measurement accuracy are expected in both cases. In the following sections, the inductive coupling effect and the capacitive coupling effect will be addressed separately and the phase correction procedures will be shown.

3. Inductive coupling in borehole EIT measurements involving two boreholes

3.1. Electromagnetic response from the subsurface

The inductive response from the subsurface during EIT field measurements comprises two parts. The first part consists of the electromagnetic response of the subsurface itself, which depends on the complex electrical resistivity distribution. The second part is associated with the magnetic field caused by the inductive coupling between the wire pairs for current injection and potential measurement. For a homogenous subsurface, the measured mutual impedance Z_m between the current and potential wires placed on the Earth's surface is given by Sunde (1968):

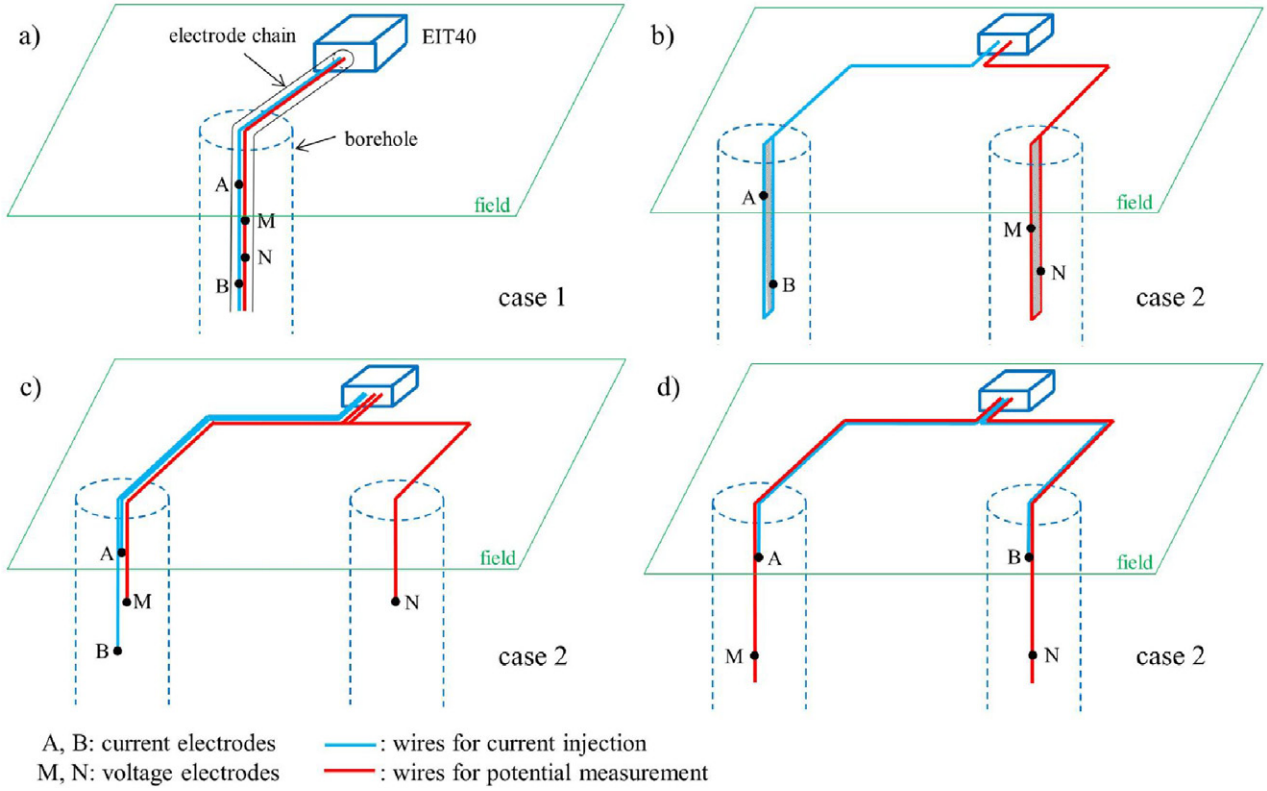

Figure 1. Case classification of EIT borehole measurements (a: single-borehole measurement; b, c, d: cross-borehole measurements).

$$Z_m = \frac{U}{I} = \int_{C_1}^{C_2}\int_{P_2}^{P_2} \frac{\partial^2 Q(r)}{\partial s \partial S} \mathrm{d}s\mathrm{d}S + \int_{C_1}^{C_2}\int_{P_1}^{P_2} P(r)\cos\varepsilon \mathrm{d}s\,\mathrm{d}S, \quad (1)$$

where $Q(r)$ is the grounding function that describes the response from the soil, C_1, C_2, P_1 and P_2 are the start and end positions of wires for current injection and potential measurement, respectively, s and S are the line elements of the wires and ε is the angle between them. The inductive contribution is described by $P(r)$:

$$P(r) = \frac{\mathrm{i}\mu\omega}{2\pi r}\left[\frac{1-(1+\gamma r)\,\mathrm{e}^{-\gamma r}}{(\gamma r)^2}\right], \quad (2)$$

where i is the imaginary unit, μ is the magnetic permeability, ω is the angular frequency, r is the distance between the wires and $\gamma = (\mathrm{i}\sigma\mu\omega)^{1/2}$ is the eddy current constant. The limit of (2) for small γ is the cable coupling:

$$P^0(r) = \frac{\mathrm{i}\mu\omega}{4\pi r}, \quad (3)$$

which only depends on the cable geometry and the frequency. In order to obtain a worst-case estimate for the influence of inductive coupling on the measured mutual impedance, we calculated the quotient between (2) and (3) for a frequency of 1 kHz, an electrical conductivity of $\sigma = 0.01\,\mathrm{S\,m^{-1}}$ and a separation between the wire segments of $r = 10\,\mathrm{m}$. The selected electrical conductivity corresponds with the highest value observed at the demonstration site Krauthausen (Vereecken *et al* 2000, Kemna *et al* 2002, Müller *et al* 2010). The maximum separation of 10 m was based on the typical borehole separations considered in field EIT studies. Using these values, the quotient P/P^0 is 0.9581–i0.0399. The imaginary part of P has the biggest effect on the phase of the measured resistivity of the soil, which is related to the real part of P/P^0. Because $\mathrm{Re}(P/P^0)$ is close to one, the influence from the subsurface is very small and it is justified to use equation (3) instead of the more complex equation (2) for typical borehole EIT applications.

Sunde (1968) also provided the two terms $Q(r)$ and $P(r)$ in (1) for a stratified subsurface:

$$\begin{aligned} Q(r) &= Q^0(r) + \mathrm{i}\omega L^0(r) \\ P(r) &= P^0(r) + P_0(\mathrm{i}\omega) \end{aligned}, \quad (4)$$

where $Q^0(r)$ reflects the resistivity of the soil and $L^0(r)$ is the earth-return inductance. $L^0(r)$ can reach a maximum value of $\mu r/4\pi$, which amounts to 10^{-6} H for $r = 10$ m (Sunde 1968). This is still negligibly small compared to the primary mutual inductance of the wires $P^0(r)/\mathrm{i}\omega$ described in (3), which is at least one order of magnitude larger. The correction term $P_0(\mathrm{i}\omega)$ due to the frequency-dependent current distribution in the earth also is very small. Since the inductive effects associated with the subsurface were found to be small and negligible, we will concentrate on the characterization and correction of the inductive coupling between the electrical wires. This means that for the correction of inductive effect only the part $P^0(r)$ must be considered, which is described in (3).

3.2. Inductive coupling between electrical wires in two boreholes

The measured transfer impedance Z_m can be calculated using (Zhao *et al* 2013):

$$Z_m = \frac{U}{I} = Z_{\text{soil}} + \mathrm{i}\omega M, \tag{5}$$

where Z_{soil} is the subsurface impedance of interest and $i\omega M$ describes the inductive cable coupling that needs to be removed from the measured data. The mutual inductance for arbitrary wire geometries can be calculated with the Neumann's integral (see e.g. Henke 2011):

$$M = \frac{\mu}{4\pi} \int_{C_1}^{C_2} \int_{P_1}^{P_2} \frac{\mathrm{d}\vec{s}\,\mathrm{d}\vec{S}}{r}, \tag{6}$$

where s and S are the infinitesimal segments of the current and potential wires and r is the distance between them. The integral paths are defined by the current electrodes C_1, C_2 and the potential electrodes P_1, P_2, respectively.

In order to derive M using (6), we must know the geometry of the wire positions exactly. Because of the small distances between the wires and the parasitic eddy currents in the shield of the electrode chain, it is very difficult to calculate the inductance M from the geometry for borehole EIT measurements with current injection and potential measurement in a single borehole chain (figure 1(*a*)). However, it is possible to use calibration measurements to remove the inductive coupling for this case since the wires are fixed inside one multicore cable (Zhao *et al* 2013). For the second case, the inductance now also depends on the layout of the two multicore electrode chains at the Earth's surface, which obviously varies with the measurement location and depends on the position of the EIT system relative to that of the boreholes. We propose to numerically model this additional inductance using Neumann's integral (6). The challenge for correcting cross-borehole EIT measurements is now to develop an effective approach that combines the calibration measurements and numerical modelling to calculate the inductive coupling for cross-borehole measurements.

3.3. The pole–pole matrix

In order to realize an effective correction method for the mutual inductance of different electrode configurations, we propose to decompose the mutual inductance of an arbitrary electrode configuration by assuming that the inductances are passive linear (reciprocal) elements. Using this assumption, the mutual inductance of electrode configuration $[C_1\, C_2\, P_1\, P_2]$ can be decomposed according to

$$M_{C_1C_2P_1P_2} = \left(M_{C_1P_1} - M_{C_1P_2}\right) - \left(M_{C_2P_1} - M_{C_2P_2}\right), \tag{7}$$

where the inductances on the right side of (7) denote the mutual inductances between the corresponding wires connected with the electrodes C_1, C_2, P_1 and P_2. The minus signs are due to the direction of the current flow and voltage within the two wire loops.

The advantage of the decomposition of the mutual inductance in (7) is that we can now formulate a pole-pole matrix that contains all mutual inductances for one electrode chain:

$$M_{8x8} = \begin{bmatrix} 0 & M_{1,2} & \cdots & M_{1,7} & M_{1,8} \\ M_{2,1} & 0 & & M_{2,7} & M_{2,8} \\ \vdots & & \ddots & & \vdots \\ M_{7,1} & M_{7,2} & & 0 & M_{7,8} \\ M_{8,1} & M_{8,2} & \cdots & M_{8,7} & 0 \end{bmatrix}, \tag{8}$$

with $M_{C,P}$ being the mutual inductance between the two wires C and P, where wire C is used for current injection and wire P is used for potential measurement. The advantage of the pole–pole matrix becomes clear when the following example is considered. For a borehole chain with eight electrodes there are a total of 840 possible electrode configurations for a four-point measurement (two current electrodes and two potential electrodes) when reciprocal measurements are considered as well. If we additionally consider 17 frequencies during borehole EIT measurements, a total of 14 280 calibration measurements would be required to correct inductive coupling effects for all possible electrode configurations. Such a calibration would be time-consuming and ineffective. In contrast, the pole-pole matrix needs only $8 \times 8 \times 17 = 1088$ calibration measurements.

The pole–pole matrix for two chains is defined as

$$\boldsymbol{M}_{16\times16} = \begin{bmatrix} \boldsymbol{M}^1 & \boldsymbol{M}^{12} \\ \boldsymbol{M}^{21} & \boldsymbol{M}^2 \end{bmatrix}, \tag{9}$$

where $\boldsymbol{M}^1$ and $\boldsymbol{M}^2$ are the pole–pole matrices of the first and second chain, respectively and $\boldsymbol{M}^{12} = (\boldsymbol{M}^{21})^T$ is the pole–pole matrix with the mutual inductances between the wires of both chains. This matrix is symmetric due to reciprocity, i.e. $M_{C,P} = M_{P,C}$. In order to consider the frequency dependency of the mutual inductance, a pole–pole matrix is defined for each frequency independently.

3.4. Determination of the pole–pole matrix

To obtain the pole-pole matrices $\boldsymbol{M}^1$ and $\boldsymbol{M}^2$ in (9), we made pole–pole calibration measurements. For this, we short-circuited all electrodes and connected them to the mass of the EIT system (figure 2). Next, current was injected at one electrode, which flowed directly back to the ground of the EIT system because of the short circuit. Simultaneously, the voltages were measured at the remaining seven electrodes. This process was repeated until all electrodes were used for current injection. The quotient of the induced voltage and the injected current is related to the mutual impedance of the two wires, but is also affected by contributions from the ground connection used for the calibration measurement and will be referred to as additive inductances in the following. These additive inductances must be removed to correctly determine the mutual inductances required in (9).

The additive inductances consist of three components for the wire segments a, b and c in figure 2. The first inductance L_a is the self-inductance of the short-circuit line from the last electrode of the chain to the ground (segment a). The second

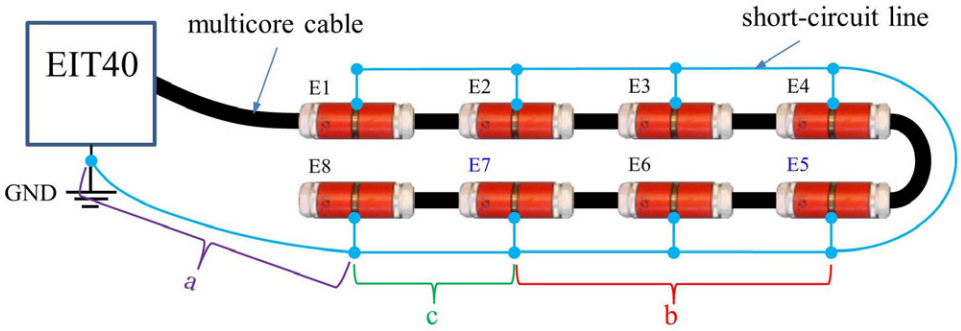

Figure 2. Pole–pole calibration measurement for electrode chain with eight ring electrodes and 25 m long multicore cable: one example for the configuration [5 7] with the segments *a*, *b*, and *c* of the short-circuit line related to the additive inductances.

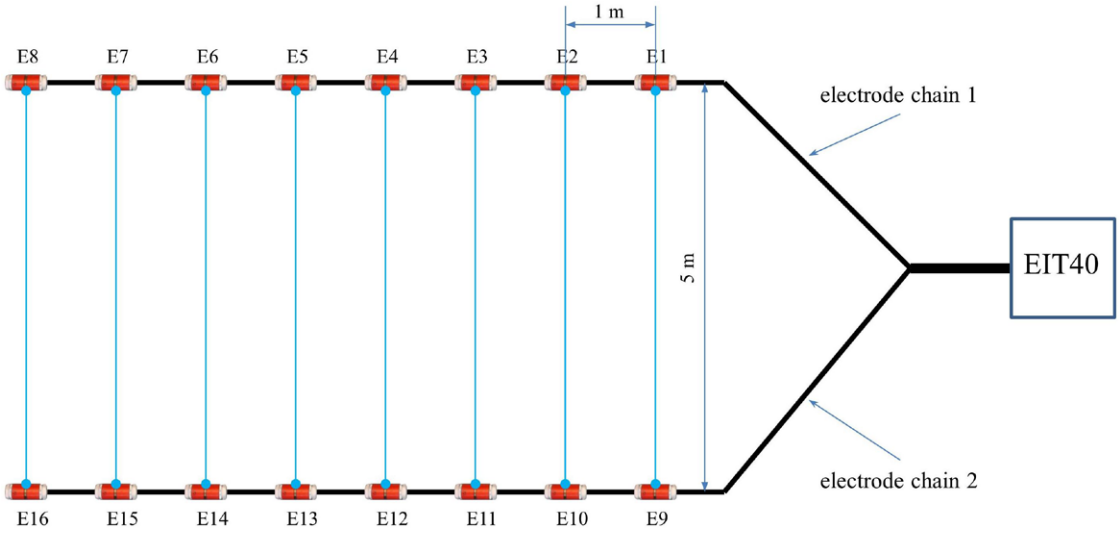

Figure 3. Measurement set-up for the calibration measurement with four-point configurations.

inductance L_b represents the mutual inductance between the wires inside the cable and the short-circuit line for segment *b* between the used current and voltage electrode. The last term L_c represents the self-inductance of the short-circuit line for segment *c* between the last electrode and the next used electrode (current or potential). For measurements with one electrode chain, a large part of these additional inductances vanishes after calculation of the mutual inductance of the electrode configuration using (7). However, for cross-hole configurations these additional inductances cannot be neglected. Thus, to ensure universal applicability they should be determined and subtracted from the mutual inductances in the pole-pole matrix. The additive inductance for each pole-pole configuration with electrodes *m* and *n* can be determined from:

$$\mathrm{ad}L_{m,n} = L_a + |s_m - s_n|\, L_b + \min(s_m, s_n)\, L_c, \qquad (10)$$

where s_m and s_n are distances from the last electrode (number 8) to the electrodes *m* and *n* normalized by the electrode separation. For the example in figure 2, the electrode configuration with current electrode 5 ($s_5 = 3$) and voltage electrode 7 ($s_7 = 1$) results in an additive inductance $\mathrm{ad}L_{5,7}$ equal to $L_a + 2L_b + L_c$.

In order to separate the additive inductances from the mutual inductance of interest, a second calibration measurement was performed using two electrode chains with electrical connection between the chains (figure 3). In contrast to the first calibration measurement with pole–pole configurations, this second set of calibration measurements uses only four-point cross-hole configurations that are unaffected by the additive inductances in (10). In particular, we connected the electrode pairs [1 9], [2 10] ... [8 16] and used these pairs as current electrodes. The remaining electrode pairs were used as potential electrodes. In order to avoid leakage of current into the subsurface, Styrofoam plates of 4 cm thickness were placed between the electrodes and the ground. We measured the transfer impedances in the frequency range of interest and transformed them into the measured mutual inductances using (7):

$$\begin{aligned} M^m_{C_1C_2P_1P_2} &= \left(M_{C_1P_1} + M_{C_2P_2}\right) - \left(M_{C_1P_2} + M_{C_2P_1}\right) + M_{EC} \\ &= \left(M^m_{C_1P_1} - \mathrm{ad}L_{C_1P_1}\right) + \left(M^m_{C_2P_2} - \mathrm{ad}L_{C_2P_2}\right) \\ &\quad - \left(M_{C_1P_2} + M_{C_2P_1}\right) + M_{EC}, \end{aligned} \qquad (11)$$

where $M^m_{C_1P_1}$ and $M^m_{C_2P_2}$ are the inductances obtained from the first pole–pole calibration measurement. The terms $\mathrm{ad}L_{C_1P_1}$

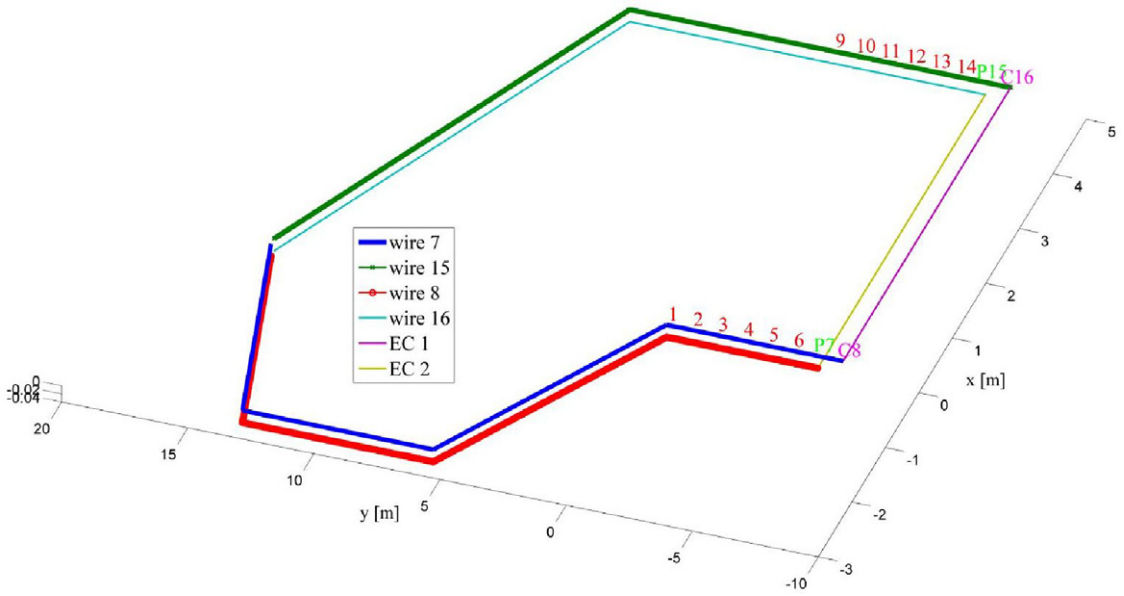

Figure 4. Segmented electrode chains for a sample configuration [8 16 7 15] using Matlab (1, 2, 3… 16: electrodes; C8, C16: current electrodes; P7, P15 potential electrodes; EC1, EC2: electrical connection).

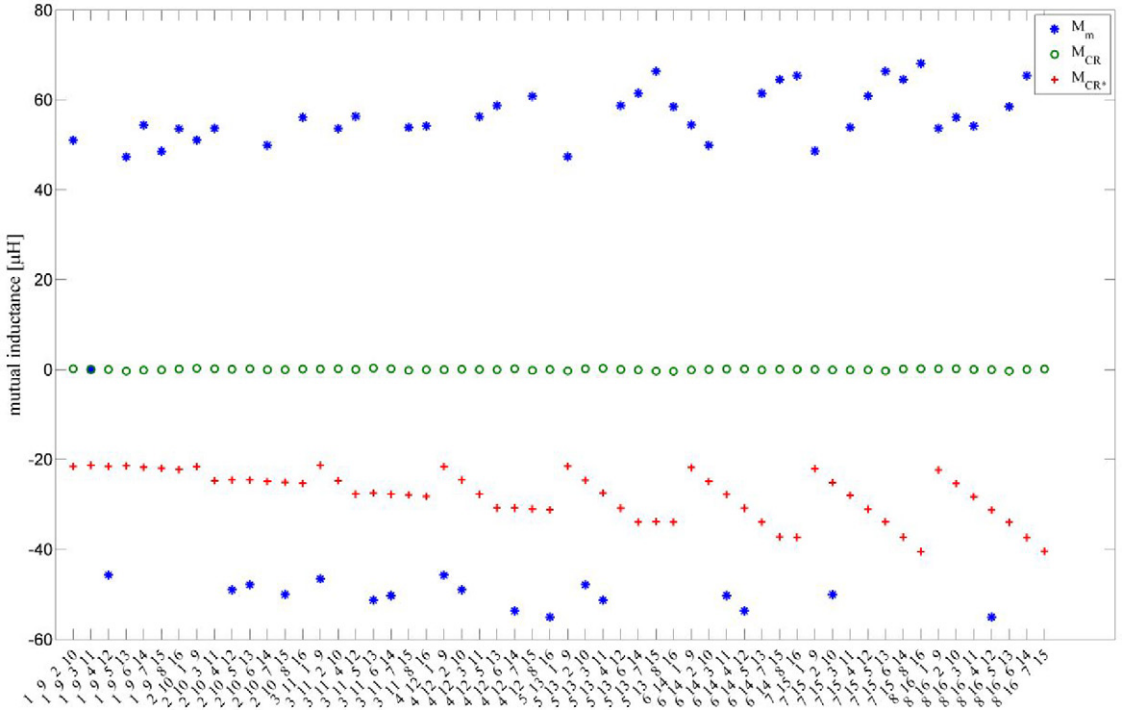

Figure 5. Comparison of the measured mutual inductance M_m (solid circles) and the calculated mutual inductance M_{CR} with (open circles) and M_{CR*} without (crosses) correction of the additive inductances of the second calibration measurement.

and ad$L_{C_2P_2}$ are the additive inductances described in (10) with the unknown parameters L_a, L_b and L_c. The terms $M_{C_1P_2}$ and $M_{C_2P_1}$ are the mutual inductances between the wires of the two chains and the term M_{EC} is the mutual inductance between the electrical connection and the wires of the electrode chains. As illustrated in figure 4, the terms$M_{C_1P_2}$, $M_{C_2P_1}$ and M_{EC} can be determined by solving (6) using the finite segment method, where the electrode chains and the electrical connection were divided into many small segments in the longitudinal direction. With this discretization, the integral (6) was converted into a summation and numerically calculated using MATLAB. Equations (10) and (11) can now be used with a set of cross-hole configurations (all configurations of figure 5) to determine L_a, L_b and L_c, because all other terms are already obtained. Because we have three unknown parameters, at least three configurations are needed to solve the resultant system of equations. However, in practice all cross-hole configurations are used to evaluate the quality of the pole–pole matrix and the calibration measurements.

Table 1. Comparison of the calculated mutual inductance M for the electrode configuration [8 16 7 15] for different geometrical errors.

Mutual inductance for configuration [8 16 7 15]		
geom. error	calc. value	Deviation
0 m	4.1445×10^{-5} H	—
0.01 m	4.1139×10^{-5} H	–0.74%
0.05 m	4.3123×10^{-5} H	3.89%
0.1 m	4.7039×10^{-5} H	11.89%
0.2 m	5.0382×10^{-5} H	17.74%
0.5 m	5.4615×10^{-5} H	24.11%

After derivation of the additive inductances, all elements of the true pole–pole matrices $\boldsymbol{M}^1$ and $\boldsymbol{M}^2$ of the electrode chains can be calculated with (10) and

$$M = M^m_{m,n} - \mathrm{ad}L_{m,n}\,. \tag{12}$$

As long as the relative positions of the electrical wires in the multicore cable do not vary with time, we only need to perform the calibration measurements once for each electrode chain. The cable layout geometry needs to be determined for each field EIT acquisition. In order to minimize the residual error after correction, we propose to use simple geometries for the cables from the system to the boreholes (e.g. triangles) so that accurate geometrical information can be obtained using a few positional measurements only.

To verify the pole–pole matrix of the mutual inductances, or rather the fitted inductances L_a, L_b and L_c, we compared the corrected mutual inductances for all electrode configurations used in the second calibration with and without the consideration of the additive inductances (figure 5). It can be seen that the differences between the measured and calculated data M_{CR*} without correction of the additive inductances are large. After consideration of the additive inductances, the measured and modelled mutual inductances match very well (deviation < 2%). These results clearly illustrate the importance of considering the additive inductances in (10).

To ensure a high accuracy of the determination of the inductances we performed a sensitivity analysis to determine how much M changes with geometrical changes in the cable layout similar to figure 3 (cable length 25 m, cable separation of the parallel part 5 m, cable length of the parallel part 9 m). Table 1 shows that the deviation between the calculated and reference mutual inductance is about 0.74% for the configuration with the largest inductive coupling ([8 16 7 15]), if the geometrical error is 0.01 m. The error is still well below 5% for a geometrical error of 0.05 m. This sensitivity analysis clearly shows that the required positional accuracy to determine the cable layout is about 0.01 m, which is feasible in most field investigations.

4. Capacitive coupling

Capacitive coupling occurs because of the potential difference between the conductive shield of the cable and the conductive subsurface and depends on the dielectric properties of the cable insulation. The geometry-dependent capacitance of the cable insulation was calculated using (Plaßmann and Schulz 2009):

$$C = 2\pi\varepsilon_0\varepsilon_r \frac{l}{\ln\frac{R_2}{R_1}}, \tag{13}$$

where ε_0 is the vacuum permittivity, R_1 and R_2 are the inner and outer radius and l is the length of the cable insulation. The relative permittivity ε_r of the cable insulation (PVC) was found to be frequency-dependent due to the slow reorientation of molecule groups with permanent dipole moment within such polymer materials (see e.g. Wagner 1914, Felger and Bassewitz 1986). Therefore, we used the Cole–Cole model (Cole and Cole 1941) to describe the complex dielectric permittivity using $\varepsilon_s = 4.79$, $\varepsilon_\infty = 3.36$, $\tau = 2.8 \times 10^{-5}$ s and $\alpha = 0.54$ (Zhao *et al* 2013). This calculation is used to determine the capacitance of cable parts which are located in the water inside the borehole. Furthermore the capacitances of the integrated amplifiers inside the electrode modules are considered. For more details about the calculation of these capacitances we refer to Zhao *et al* (2013).

These capacitances should be integrated in the forward modelling of the field EIT measurements in order to consider and remove the capacitive coupling effect. Such forward modelling can be realized using 2D or 3D meshes and the finite-element method (FEM). The calculated capacitances C of the cables should be integrated in every node of the mesh where capacitive coupling is expected. The total admittance matrix of the forward problem (Zimmermann 2011) can be obtained by adding the capacitance matrix $\boldsymbol{Y}_C = \mathrm{i}\omega C$ to the original admittance matrix

$$\boldsymbol{Y}_T = \boldsymbol{Y}_S + \boldsymbol{Y}_C\,. \tag{14}$$

Using Ohm's law, we obtain the electric potential matrix for all nodes from

$$\boldsymbol{U} = \boldsymbol{Y}_T^{-1}\boldsymbol{I}\,. \tag{15}$$

The transfer impedance and its phase shift between any two nodes (M and N) for a current injection at any nodes A and B in the mesh is obtained by

$$Z_{M,N} = U_{M,N} / I_{A,B}\,. \tag{16}$$

5. Verification of the correction methods

In order to verify the developed correction method for inductive coupling we performed EIT measurements under controlled conditions in a water-filled pool (figure 6). The pool is about 1 meter high and has a diameter of 4.5 meters. We placed the two electrode chains in the form of two overlapping rings with a diameter of 3.02 m and a chain separation of 0.5 m (figure 6(*c*)). The electrode chains were positioned using plastic floating bodies with linen strings (figures 6(*a*) and 6(*b*)). The pool was filled with tap water with a resistivity of 23 Ω m.

The transfer impedance Z for different electrode configurations was measured using the field EIT system described

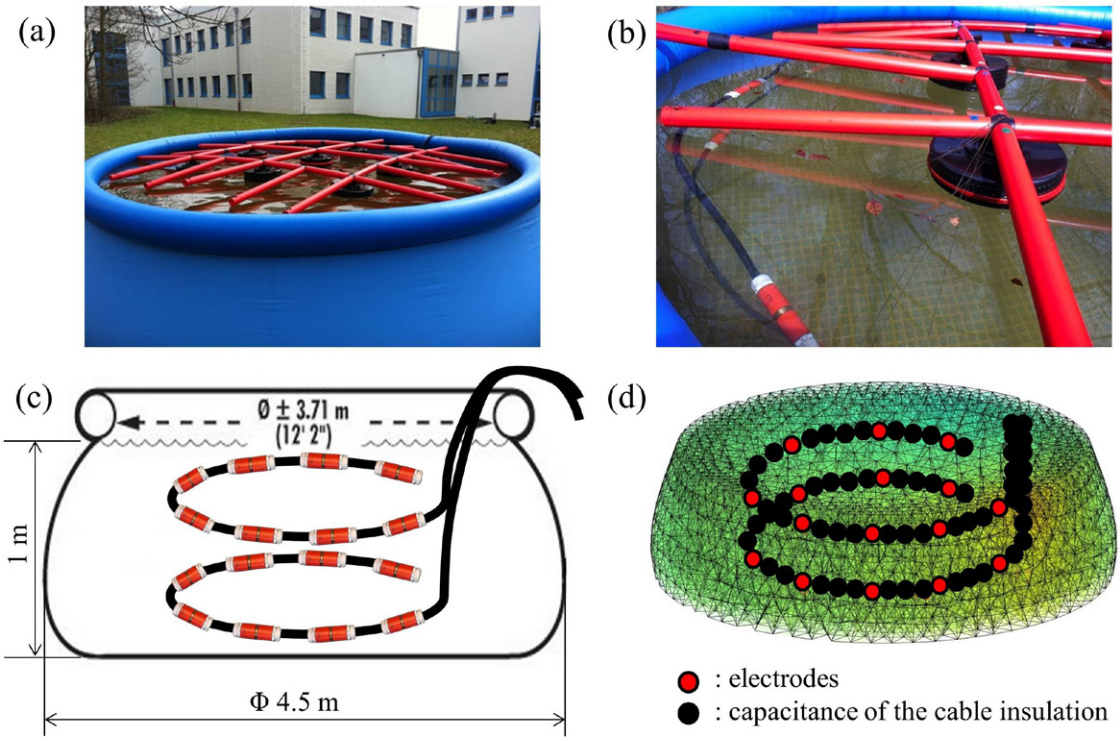

Figure 6. (*a*) Pool with floating body; (*b*) fixation of the electrode chains; (*c*) measurement set-up; (*d*) numerical modelling with 3D finite-element mesh.

above. Inductive coupling was removed from the measured impedance with the methods introduced in section 3 and the known geometry of the cables. In order to consider capacitive coupling, we generated a 3D mesh (figure 6(*d*)) with *distmesh* (Persson and Strang 2004) and calculated the admittance matrix $\boldsymbol{Y}_S$, which represents the admittances of water without capacitive effect. We determined the capacitance of the chains, the integrated amplifiers and the water-ground interface at the bottom of the pool and integrated them into the corresponding nodes of the 3D mesh (figure 6(*d*)). Using (14), (15) and (16), we calculated the theoretical transfer impedances Z_c for all electrode configurations used in the pool measurement.

Figure 7 compares the measured impedance Z, the measured impedance after correction of inductive coupling Z_{cr} and the modelled impedance considering capacitive effects Z_c for an exemplary electrode configuration. The deviation between the modelled and the measured real component of the impedances (figure 7, top) is due to the geometrical error in the modelling but it is not relevant for the phase. The remaining phase shift after correction of inductive coupling is dominated by the capacitive coupling and therefore the corrected impedance Z_{cr} should match the modelled impedance Z_c. Figure 7 (middle and bottom) shows that this comparison is indeed satisfactory. For a typical cross-hole configuration, the phase error between the corrected impedances and the modelled impedances is around 1 mrad at 1 kHz ($\varphi(Z_{cr}) = -3.4$ mrad, $\varphi(Z_c) = -2.4$ mrad). Generally, electrode configurations with large mutual inductances showed good agreement between the corrected impedances and the modelled impedances obtained from a forward model with appropriate capacitances. It is important to note that the geometry of the cables was not easy to control in the pool measurements. Thus, the positional accuracy is not high and this affected the accuracy of the modelling and the quality of the phase correction. Since it is easier to obtain the cable geometry in the case of borehole measurements, the obtained phase accuracy of 1 mrad at 1 kHz is expected to be realistic for field EIT measurements.

6. Field demonstration

Field measurements were performed at the Krauthausen test site, Germany (Vereecken *et al* 2000, Kemna *et al* 2002, Müller *et al* 2010), to demonstrate the feasibility of the correction procedures. Borehole EIT measurements were made in boreholes 75 and 76, which are separated by 5 m. The water table was at about 2 m depth. The electrode chain in borehole 75 had the first electrode at a depth of 2.8 m and the last (8th) electrode at 9.8 m. The electrode chain in borehole 76 had the first electrode at a depth of 3.2 m and the last (8th) electrode at 10.2 m. We used several electrode configurations for current injection, e.g., skip-0 (1 2, 2 3, 9 10, 10 11…), skip-2 (1 4, 2 5, 9 12, 10 13…), skip-4 (1 6, 2 7, 9 14, 10 15…), skip-6 (1 8, 9 16) and cross-hole (1 9, 2 10… 8 16, 1 11, 2 12, 5 10, 6 11, 1 16, 8 9…). For potential measurements, we used the same electrode pairs except those including the current electrodes.

We reconstructed the complex resistivity of the soil at 1 kHz using three data sets: (i) the original uncorrected measurement data, (ii) the data after correction of the inductive coupling and (iii) the data from (ii) with integrated capacitances in the FEM forward model. The complex resistivity distribution was reconstructed in 1D (z-direction) using a 3D forward model

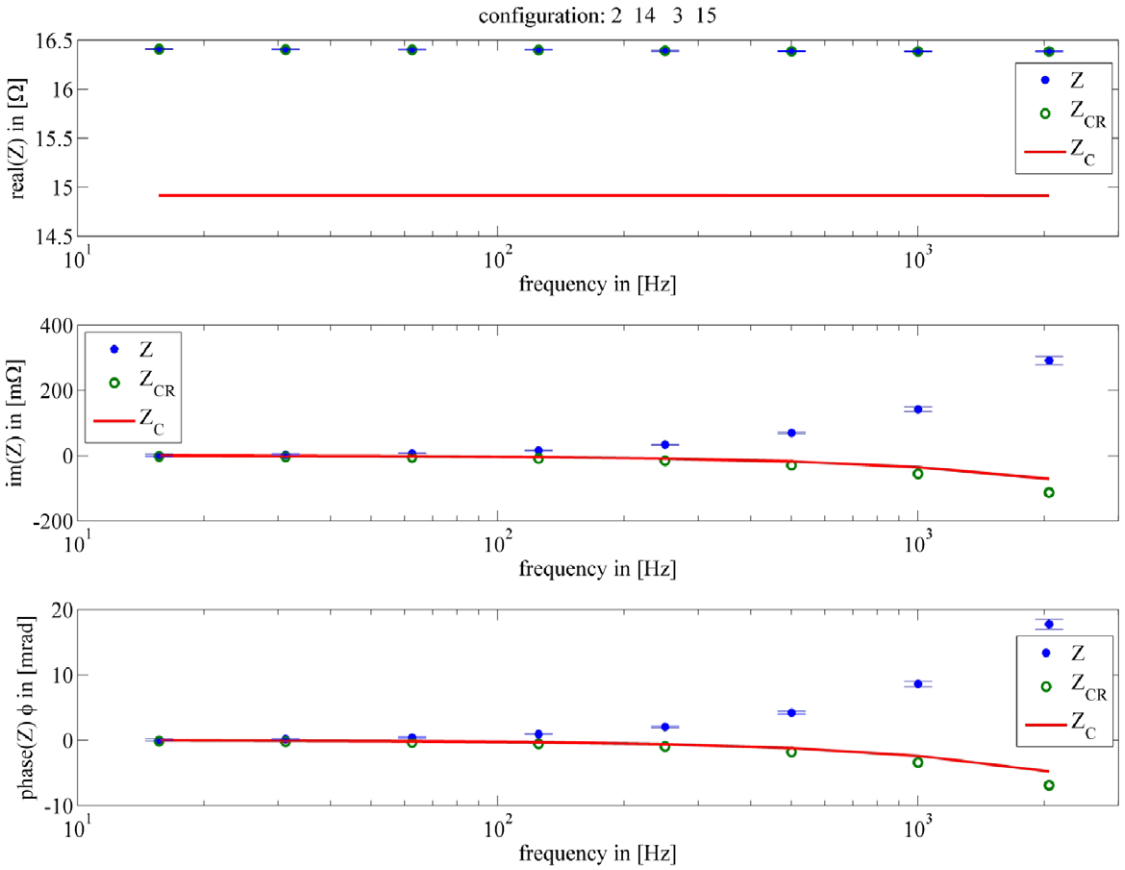

Figure 7. Comparison of the original measured impedance Z (solid circles) with error bars determined from the difference between reciprocal measurements, the impedance corrected for inductive coupling Z_{CR} (open circles) and the modelled impedance Z_C (curve) considering only the capacitive effects for an exemplary electrode configuration.

(Zimmermann *et al* 2008) of the subsurface, as already done in Zhao *et al* (2013). The regularization (smoothing) in the inversion was applied to the z-direction to obtain a smooth profile and to stabilize the reconstruction.

Figure 8 shows that the use of uncorrected impedance data resulted in excessively large phase angles and also showed physically implausible positive phase values. After the correction of inductive coupling, the phase values showed much less variation with depth and ranged from −2 to −6 mrad, which is in good agreement with laboratory measurements of the complex resistivity. The consideration of capacitive coupling only had a small effect (<1 mrad) on the inverted phase angle. As expected, the real part of the resistivity is not affected by the corrections of inductive and capacitive coupling. The retrieved resistivity profile using a 1D inversion of the cross-borehole EIT measurements are consistent with the 1D inversion results of Zhao *et al* (2013) that were obtained from EIT measurements within a single borehole.

7. Conclusions

We presented an effective approach to correct inductive coupling in borehole EIT measurements for all possible electrode configurations using one or more borehole electrode chains. This approach considers both the mutual inductance associated with inductive coupling inside each borehole chain, which is determined with calibration measurements and the mutual inductance associated with inductive coupling between two borehole chains, which is calculated from the geometry of the cable layout. These mutual inductances were assembled in a convenient pole–pole matrix that allows a simple and straightforward estimation of inductive coupling for arbitrary electrode configurations. We found that it is important to consider parasitic additive inductances of additional cables used for the calibration measurements of each chain and we developed an adapted calibration method to estimate these inductances and remove them from the mutual inductances in the pole–pole matrix. This adapted calibration method relies on a special cable layout. We also found that the inductive response from the subsurface was negligible for typical borehole EIT configurations as compared with the inductive effects of the cables. Thus, only the geometry-dependent inductive coupling of the cables was considered. The capacitive coupling between the subsurface and the cable shield is the second source of phase errors. Since this coupling depends on the (unknown) resistivity distribution of the subsurface, the effective capacitances were integrated in the forward model used in the inversion of the soil resistivity profile.

We performed pool measurements to verify the developed correction approach for inductive coupling. Electrode configurations with strong inductive coupling showed good

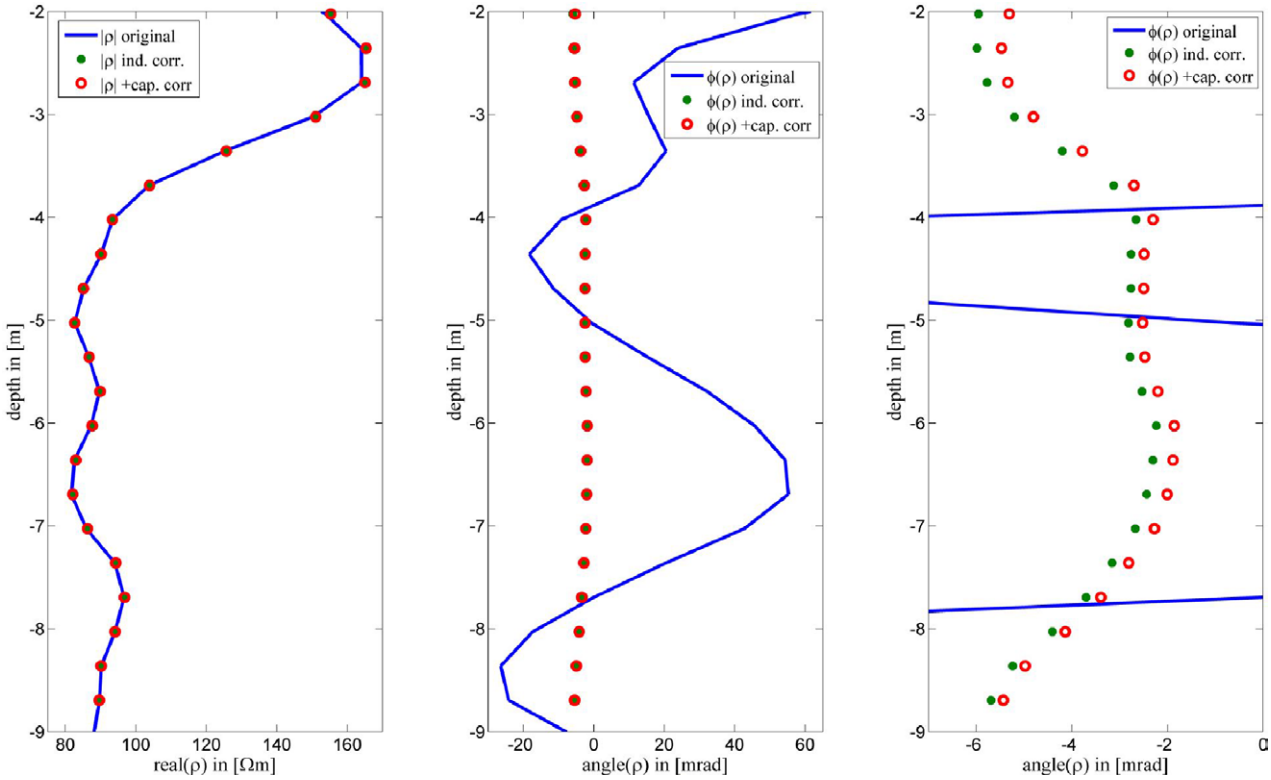

Figure 8. 1D inversion of original measured impedance (curve), impedance after correction of inductive coupling (solid circles) and impedance after correction of inductive and capacitive coupling (open circles) for cross-hole field measurements at 1 kHz (left: real part of the impedances; middle: phase angle of the impedances; right: zoom of impedance phase angles).

agreement between the corrected impedances and the calculated impedances obtained from a forward model with appropriate capacitances. The achieved phase accuracy was about 1 mrad at 1 kHz. Since positional accuracy was not optimal in these pool measurements, this accuracy is considered to be a conservative estimate of what is achievable in borehole EIT measurements. Finally, borehole EIT measurements were performed using electrode chains in two boreholes. After correction of inductive and capacitive coupling, 1D inversion results that considered cross-hole configurations were plausible and consistent with independent laboratory impedance measurements, as well as previous 1D inversion results obtained from borehole EIT measurements using a single electrode chain (Zhao *et al* 2013). The field EIT measurements clearly showed that the largest phase errors were associated with inductive coupling and that consideration of capacitive coupling was of secondary importance. Overall, the results showed that the developed correction methods are effective and applicable for field measurements in two or more boreholes. The obtained high phase accuracy considerably improves the *in situ* characterization of the frequency-dependent complex resistivity of weakly polarizable soils and sediments.

Acknowledgments

This research was supported by the project '4D Electrical Impedance Tomography' funded by the German Ministry of Education and Research (BMBF) in the framework of the R&D Program GEOTECHNOLOGIEN (grant 03G0743B). We would like to thank the two anonymous reviewers for their comments that helped to improve the manuscript.

References

Binley A, Slater L D, Fukes M and Cassiani G 2005 Relationship between spectral induced polarization and hydraulic properties of saturated and unsaturated sandstone *Water Resources Res.* **41** W12417

Breede K, Kemna A, Esser O, Zimmermann E, Vereecken H and Huisman J A 2012 Spectral induced polarization measurements on variably saturated sand-clay mixtures *Near Surf. Geophys.* **10** 479–89

Cole K S and Cole R H 1941 Dispersion and absorption in dielectrics I. Alternating current characteristics *J. Chem. Phys.* **9** 341–51

Felger H K and Bassewitz A 1986 *Polyvinylchlorid Kunststoffhandbuch* vol 2 (München: Hanser)

Flores Orozco A, Kemna A, Oberdörster C, Zschornack L, Leven C, Dietrich P and Weiss H 2012 Delineation of subsurface hydrocarbon contamination at a former hydrogenation plant using spectral induced polarization imaging *J. Contam. Hydrol.* **136–137** 131–44

Henke H 2011 *Elektromagnetische Felder* (Berlin: Springer)

Kemna A, Binley A, Ramirez A and Daily W 2000 Complex resistivity tomography for environmental applications *Chem. Eng. J.* **77** 11–8

Kemna A, Kulessa B and Vereecken H 2002 Imaging and characterisation of subsurface solute transport using electrical resistivity tomography (ERT) and equivalent transport models *J. Hydrol.* **267** 125–46

Leroy P, Revil A, Kemna A, Cosenza P and Ghorbani A 2008 Complex conductivity of water-saturated packs of glass beads *J. Colloid Interface Sci.* **321** 103–17

Müller K, Vanderborght J, Englert A, Kemna A, Huisman J A, Rings J and Vereecken H 2010 Imaging and characterization of solute transport during two tracer tests in a shallow aquifer using electrical resistivity tomography and multilevel groundwater samplers *Water Resources Res.* **46** W03502

Persson P-O and Strang G 2004 A simple mesh generator in MATLAB *SIAM Rev.* **46** 329–45

Plaßmann W and Schulz D 2009 *Handbuch Elektrotechnik* (Wiesbaden: Vieweg Teubner GWV Fachverlage)

Slater L D and Lesmes D 2002 IP interpretation in environmental investigations *Geophysics* **67** 77–88

Sunde E D 1968 *Earth Conduction Effects In Transmission Systems* (New York: Dover)

Vanhala H 1997 Mapping oil-contaminated sand and till with the spectral induced polarization (SIP) method *Geophys. Prospect.* **45** 303–26

Vereecken H, Döring U, Hardelauf H, Jaekel U, Hashagen U, Neuendorf O, Schwarze H and Seidemann R 2000 Analysis of solute transport in a heterogeneous aquifer: the Krauthausen field experiment *J. Contam. Hydrol.* **45** 329–58

Wagner K 1914 Dielektrische Eigenschaften von verschiedenen Isolierstoffen *Archiv für Elektrotechnik* **3** 67–106

Wait J R 1984 Electromagnetic response of a discretely grounded circuit *Geophysics* **49** 577–80

Ward S H and Hohmann G W 1988 Electromagnetic theory for geophysical applications *Electromagnetic Methods in Applied Geophysics* ed M N Nabighian (Tulsa, OK: Society of Exploration Geophysicists)

Wynn J C and Zonge K L 1977 Electromagnetic coupling *Geophys. Prospect.* **25** 29–51

Zhao Y, Zimmermann E, Huisman J A, Treichel A, Wolters B, Waasen S V and Kemna A 2013 Broadband EIT borehole measurements with high phase accuracy using numerical corrections of electromagnetic coupling effects *Meas. Sci. Technol.* **24** 085005

Zimmermann E 2011 Phasengenaue Impedanzspektroskopie und -tomographie für geophysikalische Anwendungen *PhD Thesis* Rheinische Friedrich–Wilhelms–Universität Bonn

Zimmermann E, Huisman J A, Kemna A, Berwix J, Glaas W, Meier H, Wolters B and Esser O 2010 Advanced electrical impedance tomography system with high phase accuracy *6th World Congress on Industrial Process Tomography (WCIPT6) (6–9 September 2010, Beijing)* pp 583–91

Zimmermann E, Kemna A, Berwix J, Glaas W and Vereecken H 2008 EIT measurement system with high phase accuracy for the imaging of spectral induced polarization properties of soils and sediments *Meas. Sci. Technol.* **19** 094010